Resonant and Inelastic Andreev Tunneling Observed on a Carbon Nanotube Quantum Dot

J. Gramich, A. Baumgartner,* and C. Schönenberger
Department of Physics, University of Basel, Klingelbergstrasse 82, CH-4056 Basel, Switzerland
(Received 1 July 2015; published 16 November 2015)

We report the observation of two fundamental subgap transport processes through a quantum dot (QD) with a superconducting contact. The device consists of a carbon nanotube contacted by a Nb superconducting and a normal metal contact. First, we find a single resonance with position, shape, and amplitude consistent with the theoretically predicted resonant Andreev tunneling (AT) through a single QD level. Second, we observe a series of discrete replicas of resonant AT at a separation of ~145 μeV, with a gate, bias, and temperature dependence characteristic for boson-assisted, inelastic AT, in which energy is exchanged between a bosonic bath and the electrons. The magnetic field dependence of the replica's amplitudes and energies suggest that two different bosons couple to the tunnel process.

DOI: 10.1103/PhysRevLett.115.216801 PACS numbers: 73.23.-b, 74.45.+c

Electron transport in nanostructures with superconducting (S) and normal metal (N) contacts have attracted considerable attention recently, because of the discovery of new transport processes and exotic quantum mechanical states of matter. While S contacts have been used in bias spectroscopy for many years, transport in nanostructures at energies below the superconductor's energy gap became relevant only recently, for example, in the search for solid-state versions of Majorana fermions [1], Cooper pair splitting [2–5], or the study of Andreev bound states (ABSs) [6–9].

The most fundamental low-energy transport process between an N and an S reservoir is Andreev reflection, in which an electron from N can only enter S by forming a Cooper pair with a second electron of opposite spin and momentum (for a standard s-wave superconductor). This process is slightly more complicated if the two reservoirs are connected by a quantum dot (QD), in which the charging energy suppresses a double occupation. The resulting resonant Andreev tunneling (resonant AT) is illustrated in Fig. 1(a) as an intuitive sequential tunneling process. At zero bias the two electrons forming a Cooper pair tunnel through the QD at the same energy, which leads to a peak in the differential conductance G. At a finite bias, resonant AT is allowed only for electrons with energies aligned to the electrochemical potential μ_S of S, i.e., only if the QD resonance (μ_{QD}) is aligned to μ_S; see Fig. 1(a). Resonant AT can be identified by the distinctive resonance line shape with a sharper decay than when tunneling into a normal reservoir [10–12].

An additional transport process is boson-assisted tunneling, in which bosons from the environment are absorbed or emitted in an inelastic tunneling process. This mechanism leads to replicas of the elastic tunnel process at higher energies. For example, in carbon nanotubes (CNTs) with normal metal contacts, phonons can result in additional resonances [13] and even in the suppression of the current for strong electron-phonon couplings (Franck-Condon blockade) [14]. Also, the electromagnetic environment can provide energy for photon-assisted processes, resulting in discrete QD resonance side bands [15,16]. Phonon [17] and photon [18] induced discrete replicas of elastic AT were predicted recently for QDs with an S contact. Such inelastic AT is illustrated in Fig. 1(b): a Cooper pair can only be

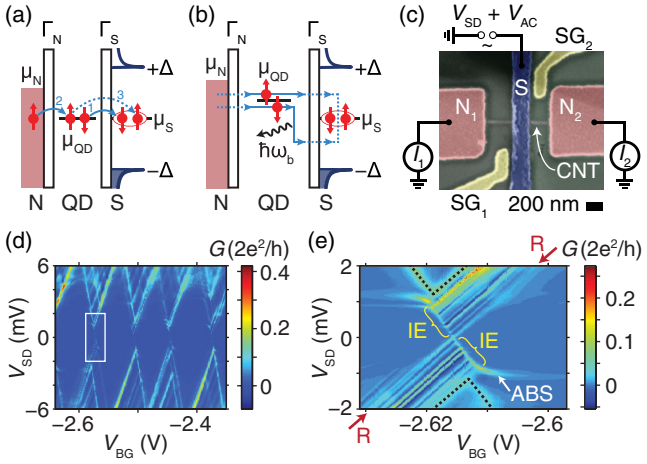

FIG. 1 (color online). (a) Schematic of resonant AT. Two electrons tunnel through the QD into S for $\mu_{QD} = \mu_S$ and $\mu_N > \mu_{QD}$. (b) Schematic of inelastic AT. Two electrons tunnel through the QD into S at $\mu_{QD} = \mu_S + (n/2)\hbar\omega_b$ for $\mu_N > \mu_{QD}$ by emitting multiples of the energy $\hbar\omega_b$ to the environment. (c) SEM image of a representative device and schematic of the measurement setup. (d) Differential conductance of QD1 as function of V_{SD} and V_{BG}. (e) Detailed conductance map of the region indicated in (d). The resonant and inelastic AT lines are labeled R and IE, respectively. The dotted lines point out the Coulomb blockade diamond edges and ABS an Andreev bound state.

formed by two electrons of opposite energy with respect to the chemical potential of S, μ_S. If the QD level is aligned at a positive energy, both electrons traverse the QD at the same energy, and, to form a Cooper pair, one relaxes the energy $\hbar\omega_b$ to the environment with a bosonic excitation spectrum. As is evident from Fig. 1(c) this condition is met at $\mu_{QD} - \mu_S = (n/2)\hbar\omega_b (n \in \mathbb{N})$, in contrast to twice this value in boson-assisted processes in devices with normal contacts. Neither resonant nor inelastic AT have been observed in QDs before, probably because both require the QD resonance width to be much smaller than the superconducting energy gap, Δ.

Here we use a CNT quantum dot contacted by a superconducting Nb and a normal metal contact to investigate a discrete subgap resonance fully consistent with resonant AT. In addition, the resonance has multiple, very sharp replicas due to inelastic boson-assisted AT. Nb shows a large energy gap in CNT devices [9,19], in our case up to 1.2 meV, which allows us to perform bias spectroscopy in the regime of the QD lifetime broadening being considerably smaller than Δ, which is crucial to identify these processes.

Figure 1(c) shows a false color scanning electron microscopy (SEM) image, including a schematic of the measurement setup. The CNTs were grown by chemical vapor deposition (CVD) on a Si^{++}/SiO_2 substrate used as a back gate. Subsequently, the surface is treated by an rf-induced hydrogen plasma, similar to Refs. [9,20]. In this process about 30% of the CNTs are etched away, which probably serves as a selection process for defect-free clean CNTs. On a suitable CNT we fabricate a central ~200 nm wide and ~2 mm long Ti/Nb (3 nm/40 nm) contact (S) and two normal metal Ti/Au (5/65 nm) contacts (N) on either side of S at a distance of ~300 nm, in a Cooper pair splitter geometry [5] with side gates (SGs) for individual electrical tuning of the two CNT sides. Between the contacts two separate QDs form, but no signals could be found that depend on both QDs [21]. Here we focus solely on experiments on QD1. The experiments were carried out in a dilution refrigerator at a base temperature of ~110 mK. In Fig. 1(d) the differential conductance G through QD1 is plotted as a function of the back gate voltage, V_{BG}, and the bias applied to S, V_{SD}. We find very clear Coulomb blockade (CB) diamonds with an addition energy of ~6.6 meV, a level spacing of ~1.2 meV, and a well-defined superconducting gap of ~1.2 meV, which separates the CB diamonds in a characteristic way due to the gap in the single-particle density of states in the S contact [21]. This gap is reduced monotonically with a magnetic field B applied perpendicular to the CNT and the substrate and vanishes at $B \approx 1.5$ T [21]. Figure 1(e) shows G plotted in the region indicated by the rectangle in Fig. 1(d). Here we find up to 7 weak but very sharp parallel resonance lines with the same positive slope as the CB diamonds. Similar features appear in all other CB diamonds [21], independent of the QD charge state. The average spacing between the lines is $\sim 145 \pm 30$ μeV, with some resonances showing significant deviations from this value. Only one of these parallel lines (R) crosses the entire transport gap, while the other lines (IE) end at a finite subgap bias. Pronounced negative differential conductance (NDC) values occur between the conductance maxima. An additional structure arises due to an Andreev bound state [labeled ABS in Fig. 1(e)], which leads to some amplitude modulation, but will not be discussed in more detail here. Line R we identify with resonant AT. To demonstrate this, we compare the line shape of the zero-bias CB resonance measured in the normal state at $B = 5$ T shown in Fig. 2(a) to the resonance at zero field, i.e., in the superconducting phase of S, which is plotted in Fig. 2(b). For the following fits we added an identical background determined by the data points far off resonance (not shown). In the normal state we expect a Breit-Wigner (BW) line shape due to lifetime broadening, which is described by $G(\Delta V_{BG}) = (e^2/h)[\Gamma_1\Gamma_2/(\Delta E^2 + \Gamma^2/4)]$, with $\Gamma = \Gamma_1 + \Gamma_2$ and the QD level detuning $\Delta E = -e\alpha(\Delta V_{BG} - V_{BG}^{(0)})$, where α is the lever arm of the back gate to the QD and $V_{BG}^{(0)}$ the position of the resonance. This expression fits the observed line shape in Fig. 2(a) very well (blue curve) for the tunnel coupling parameters $\Gamma_1 \approx 9.0$ and $\Gamma_2 \approx 96.5$ μeV. As a comparison, we also plot the best fit using the expression for thermally broadened resonances (dotted green line), $G = (e^2/h)(1/4k_BT)(\Gamma_1\Gamma_2/\Gamma)\cosh^{-2}(\Delta E/2kT)$, which does not describe the data well. For resonant AT in the limit of noninteracting electrons the expected line shape is

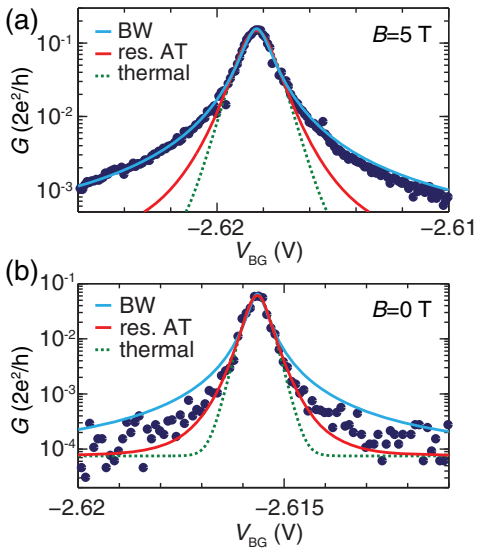

FIG. 2 (color online). Resonance line shapes: G as function of V_{BG} (points) at zero bias (a) in the normal state at $B = 5$ T and (b) at zero field in the superconducting state. The blue, red, and dotted green lines are best fits to the data using the expressions for a Breit-Wigner (BW), resonant AT, and a thermally broadened QD resonance, respectively.

$G = (2e^2/h)[2\Gamma_1\Gamma_2/(4\Delta E^2 + \Gamma_1^2 + \Gamma_2^2)]^2$ [10,12], which also deviates strongly from the data. In contrast, the resonance at zero magnetic field plotted in Fig. 2(b) is described best by the expression for resonant AT: the measured conductance values decay faster away from the maximum than in the normal state. The extracted values for the tunnel coupling using the BW expression are a factor of 3–7 smaller than in the normal state, while the values extracted from the resonant AT expression, $\Gamma_1 \approx 8.4$ μeV and $\Gamma_2 \approx 66.5$ μeV, are very similar to the ones in the normal state. We find similar values also in gate sweeps at a small bias [21]. From the line shapes and the observation that this resonance occurs when the QD level is aligned to the electrochemical potential of S, we conclude that resonance R running through the full energy gap of the superconductor is due to resonant AT.

The replicas (IE) parallel to the resonant AT line (R) found in Fig. 1(e) we attribute to the emission and absorption of energy from or into a bosonic reservoir in an inelastic Andreev tunneling process. The bias condition for this process [see Fig. 1(b)] is $\mu_S < \mu_{QD} < \mu_N$ [17,21], which results in the lines ending at a finite subgap bias, as observed in Fig. 1(e). Following the predictions of Ref. [17] for phonons, Fig. 3 shows a series of back gate sweeps obtained at different temperatures. The zero-bias curves in Fig. 3(a) are symmetric with respect to the central resonant AT peak indicated by the black arrow. The amplitude of this peak is reduced considerably with increasing temperature, while the width increases because of side peaks (red arrows) emerging as weak shoulders between 0.5 and 1 K. The amplitudes of the indicated features are plotted in the inset of Fig. 3(a) for the three temperatures, which shows that resonant AT is reduced with increasing temperature ($\sim 1/k_B$T) due to the thermal broadening of the Fermi functions in the normal metal contact. In contrast, the absorption side peaks increase in amplitude at higher temperatures due to the thermal population of the boson states [28], in good qualitative agreement with the predictions for phonon-assisted AT [17,29].

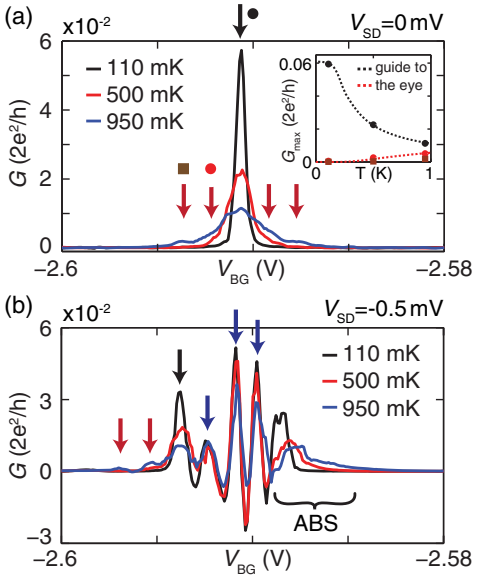

FIG. 3 (color online). Temperature dependence of resonant and inelastic AT. Differential conductance G as function of V_{BG} at (a) $V_{SD} = 0$ and (b) $V_{SD} = -0.5$ mV for the three indicated temperatures. The black arrow points out the resonant AT line, the red arrows the boson-absorbing and the blue arrows the boson-emitting resonances [21]. The inset in Fig. (a) shows the peak amplitudes of the features indicated in the main figure.

Back gate sweeps at the bias $V_{SD} = -0.5$ mV are plotted in Fig. 3(b) for the same temperatures, which again shows the reduction of the resonant AT amplitude (black arrow) and the onset of boson-assisted inelastic AT at more negative gate voltages (red arrows). At more positive voltages, i.e., $\mu_S < \mu_{QD}$, resonances occur with slightly decreasing amplitudes and essentially constant widths (blue arrows) [21]. In addition, we observe pronounced negative differential conductance (NDC) between the peaks. All these findings are in very good qualitative agreement with inelastic AT in which the excess energy of the tunneling electrons is emitted into a bosonic bath [17]. In particular, the resonance width in this process is mainly determined by the tunnel couplings, which we do not expect to change greatly with temperature. NDC is also expected, since the resonance condition is determined by the QD level position and not by the Fermi energy of the normal metal lead, which leads to peaks in the current and a peak-dip structure in the differential conductance.

We now investigate the resonant and inelastic AT as a function of an external magnetic field B applied perpendicular to the substrate plane. Figure 4(a) shows G as a function of V_{SD} and B at the back gate voltage at which the elastic AT resonance (R) crosses $V_{SD} = 0$. We find that the energy gap detected by the QD shrinks monotonically up to ~0.3 T and is then roughly constant up to ~1 T and disappears around 1.5 T [21]. Here we focus only on the subgap features: the resonant AT line R is essentially unaffected at fields below $B \approx 0.7$ T and splits at higher fields due to Zeeman shifts of the resonances. These do not affect the following analysis since we extract all values directly from Coulomb diamond experiments [21]. We can visualize the transition from resonant AT to a Breit-Wigner characteristics with increasing field by plotting the extracted tunnel parameter, $\Gamma = \Gamma_1 + \Gamma_2$, as a function of B, which is shown in Fig. 4(b). We assume that the tunnel couplings stay roughly constant with increasing B [21]. While up to $B \approx 1$ T the expression for resonant AT reproduces nicely the large-field values of the BW fit (light red band), it overestimates the coupling by more than a factor of 2 at high fields. At intermediate fields between 1 and 3 T both line shapes deviate considerably from the expected values, which suggests that normal electron tunneling and AT coexist at fields where the visible transport gap is reduced to zero.

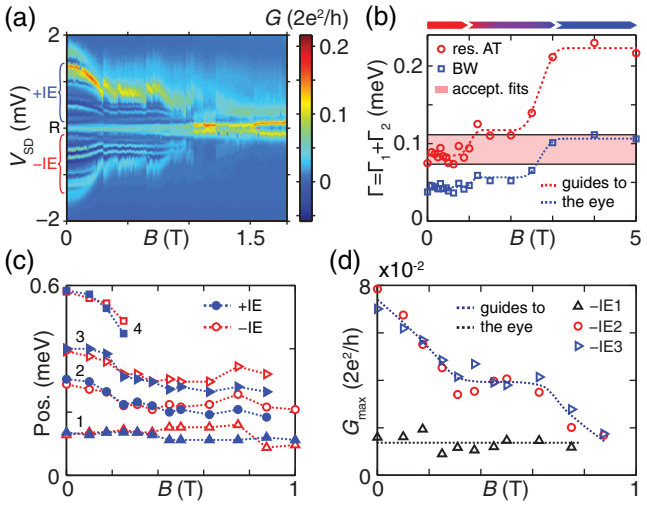

FIG. 4 (color online). Magnetic field dependence of resonant and inelastic AT. (a) G as a function of the bias V_{SD} and the external magnetic field B at a fixed back gate voltage where the resonance R crosses $V_{SD} = 0$. (b) Tunnel coupling $\Gamma = \Gamma_1 + \Gamma_2$ of resonance R extracted from the resonant AT and the Breit-Wigner expressions as a function of B. The fits are obtained from color scale images at the same relative position [21]. (c) Energy and (d) amplitude of the inelastic AT peaks (IE) as a function of B. The resonances are labeled in (c) for increasing energy.

Figures 4(c) and 4(d) show the magnetic field dependence of the position (energy) and the peak amplitude of the inelastic AT lines, respectively, extracted from CB spectroscopy [21]. We plot the position of the conductance maxima relative to the resonance R at negative and positive bias up to 1 T and label the lowest resonances in energy in Fig. 4(c). While the energy of resonance IE1 is essentially constant in this field interval, the positions of IE2, IE3, and IE4 are all reduced and scale similarly with increasing field, but not linearly with the energy gap [21]. For the latter resonances the spacing stays roughly constant. Even more pronounced is the difference in the field dependence of the resonance amplitudes, plotted in Fig. 4(d): the amplitude of IE1 is independent of B within experimental error, but the amplitudes of IE2 and IE3 decay continuously on the scale of 1 T.

Inelastic AT is mediated by the absorption or emission of bosons. In our system, three types of bosons might be responsible for these subgap processes: (i) phonons, e.g., mechanical oscillations in the CNT [17], where the longitudinal acoustic modes in the doubly clamped CNT, or the CNT squash mode [30] can yield quantized energies of the observed energy scale. (ii) Plasma modes in the millimeter scale superconducting contact [31]. (iii) Photons, i.e., electromagnetic modes of the resonator formed by the inductance and capacitance of the S contact, which are damped by Ohmic dissipation in normal metals. Phonons naturally account for the temperature dependence of the inelastic AT lines, but it is not straightforward to explain a magnetic field dependence. Photons account, at least qualitatively, for the field and temperature dependence, since the kinetic inductance L_k of S diverges with decreasing energy gap, which results in a reduced resonance frequency $\propto (L_k C)^{-1/2}$ (C is the capacitance to the back gate) [32]. The fact that we find qualitatively different magnetic field characteristics for the lowest energy inelastic AT peak compared to the resonances at higher energies might indicate that two different bosonic baths are coupled to our QD.

In summary, the large superconducting transport gap found in our Nb-contacted CNT QDs and the sharp QD resonances allow us to identify resonant (elastic) and inelastic Andreev tunneling in a QD-superconductor structure. In addition, we also demonstrate the impact of the energy gap on the CB diamond structure. The temperature dependence of the inelastic replicas of resonant AT is consistent with bosonic excitations that open additional transport channels. However, from our experiments the nature of the bosons is difficult to assess. The magnetic field dependence might even hint at the possibility of two different bosonic systems coupling to the QD. Our experiments demonstrate that, in contrast to normal metal systems, such excitations can become the dominant transport mechanisms in S-QD systems, while a smearing of the discrete resonances is a possible origin of the heavily discussed "soft gaps" [33] in large-gap superconductor nanostructures. In addition, the coupling to bosonic reservoirs is also expected to result in replicas of other subgap features, for example, ABSs [34]. Similar devices with engineered bosonic environments could shed more light on the nature of the observed processes and lead to hybrid quantum systems with a controlled coupling to the superconductor. For example, novel techniques allow the fabrication of suspended CNTs with superconducting and other contact materials [35], which should give access to well-controlled CNT phonons [36]. Using the same technique, a radio-frequency cavity can be coupled to the CNT QD, which results in a well-controlled electromagnetic environment with discrete modes [37].

We thank C. Stampfer and S. Csonka for helpful discussions and J. Schindele and M. Weiss for their support in the laboratory. We also gratefully acknowledge the financial support by the EU FP7 project SE^{2}ND, the EU ERC project QUEST, the Swiss NCCR Quantum and the Swiss SNF.

*andreas.baumgartner@unibas.ch

[1] V. Mourik, K. Zuo, S. M. Frolov, S. R. Plissard, E. P. A. M. Bakkers, and L. P. Kouwenhoven, Science **336**, 1003 (2012).

[2] L. Hofstetter, S. Csonka, J. Nygård, and C. Schönenberger, Nature (London) **461**, 960 (2009).

[3] L. G. Herrmann, F. Portier, P. Roche, A. L. Yeyati, T. Kontos, and C. Strunk, Phys. Rev. Lett. **104**, 026801 (2010).
[4] L. Hofstetter, S. Csonka, A. Baumgartner, G. Fülöp, S. d'Hollosy, J. Nygård, and C. Schönenberger, Phys. Rev. Lett. **107**, 136801 (2011).
[5] J. Schindele, A. Baumgartner, and C. Schönenberger, Phys. Rev. Lett. **109**, 157002 (2012).
[6] J.-D. Pillet, C. H. L. Quay, P. Morfin, C. Bena, A. Levy Yeyati, and P. Joyez, Nat. Phys. **6**, 965 (2010).
[7] T. Dirks, T. L. Hughes, S. Lal, B. Uchoa, Y.-F. Chen, C. Chialvo, P. M. Goldbart, and N. Mason, Nat. Phys. **7**, 386 (2011).
[8] E. J. H. Lee, X. Jiang, M. Houzet, R. Aguado, C. M. Lieber, and S. De Franceschi, Nat. Nanotechnol. **9**, 79 (2013).
[9] J. Schindele, A. Baumgartner, R. Maurand, M. Weiss, and C. Schönenberger, Phys. Rev. B **89**, 045422 (2014).
[10] C. W. J. Beenakker, Phys. Rev. B **46**, 12841 (1992).
[11] Q.-f. Sun, J. Wang, and T.-h. Lin, Phys. Rev. B **59**, 3831 (1999).
[12] Y. Zhu, Q.-f. Sun, and T.-h. Lin, Phys. Rev. B **64**, 134521 (2001).
[13] S. Sapmaz, P. Jarillo-Herrero, Ya. M. Blanter, C. Dekker, and H. S. J. van der Zant, Phys. Rev. Lett. **96**, 026801 (2006).
[14] R. Leturcq, C. Stampfer, K. Inderbitzin, L. Durrer, C. Hierold, E. Mariani, M. G. Schultz, F. von Oppen, and K. Ensslin, Nat. Phys. **5**, 327 (2009).
[15] W. G. van der Wiel, T. H. Oosterkamp, S. de Franceschi, C. J. P. M. Harmans, and L. P. Kouwenhoven, NATO Science Series **72**, 43 (2002).
[16] C. Meyer, J. M. Elzerman, and L. P. Kouwenhoven, Nano Lett. **7**, 295 (2007).
[17] S.-N. Zhang, W. Pei, T.-F. Fang, and Q.-F. Sun, Phys. Rev. B **86**, 104513 (2012).
[18] Q.-f. Sun, J. Wang, and T.-h. Lin, Phys. Rev. B **59**, 13126 (1999).
[19] M. Gaass, S. Pfaller, T. Geiger, A. Donarini, M. Grifoni, A. K. Hüttel, and C. Strunk, Phys. Rev. B **89**, 241405(R) (2014).
[20] R. Yang, L. Zhang, Y. Wang, Z. Shi, D. Shi, H. Gao, E. Wang, and G. Zhang, Adv. Mater. **22**, 4014 (2010).
[21] See Supplemental Material http://link.aps.org/supplemental/10.1103/PhysRevLett.115.216801, which includes Refs. [22–27], a discussion of the gate and bias dependence of the transport processes, additional measurements, and details of the data analysis.
[22] S. Datta, *Electronic Transport in Mesoscopic Systems* (Cambridge University Press, Cambridge, England, 1995).
[23] T. Ihn, *Semiconductor Nanostructures: Quantum States and Electronic Transport* (Oxford University Press, New York, 2010).
[24] R. Deblock, E. Onac, L. Gurevich, and L. P. Kouwenhoven, Science **301**, 203 (2003).
[25] R. Barends, J. Wenner, M. Lenander, Y. Chen, R. C. Bialczak, J. Kelly, E. Lucero, P. O'Malley, M. Mariantoni, D. Sank, H. Wang, T. C. White, Y. Yin, J. Zhao, A. N. Cleland, J. M. Martinis, and J. J. A. Baselmans, Appl. Phys. Lett. **99**, 113507 (2011).
[26] C. C. Escott, F. A. Zwanenburg, and A. Morello, Nanotechnology **21**, 274018 (2010).
[27] R. Flükiger, S. Y. Hariharan, R. Künzler, H. L. Luo, F. Weiss, T. Wolf, and J. Q. Xu, *Landolt-Börnstein—Group III Condensed Matter*, Springer Materials (Springer-Verlag GmbH, New York, 1993).
[28] The conductance maximum is expected to scale with temperature as $\sim 1/k_B T[e^{\hbar\omega_b/k_B T} - 1]^{-1}$.
[29] We note that the gate voltage, bias, and temperature dependence is quite different for boson-assisted quasiparticle tunneling, which is discussed in the Supplemental Material [21].
[30] M. S. Dresselhaus, G. Dresselhaus, R. Saito, and A. Jorio, Phys. Rep. **409**, 47 (2005).
[31] B. Camarota, F. Parage, F. Balestro, P. Delsing, and O. Buisson, Phys. Rev. Lett. **86**, 480 (2001).
[32] K. Watanabe, K. Yoshida, T. Aoki, and S. Kohjiro, Jpn. J. Appl. Phys. **33**, 5708 (1994).
[33] J. P. Pekola, V. F. Maisi, S. Kafanov, N. Chekurov, A. Kemppinen, Yu. A. Pashkin, O.-P. Saira, M. Möttönen, and J. S. Tsai, Phys. Rev. Lett. **105**, 026803 (2010).
[34] J. Baránski and T. Dománski, J. Phys. Condens. Matter **27**, 305302 (2015).
[35] J. Gramich, A. Baumgartner, M. Muoth, C. Hierold, and C. Schönenberger, Phys. Status Solidi B (2015).
[36] A. Benyamini, A. Hamo, S. V. Kusminskiy, F. von Oppen, and S. Ilani, Nat. Phys. **10**, 151 (2014).
[37] V. Ranjan, G. Puebla-Hellmann, M. Jung, T. Hasler, A. Nunnenkamp, M. Muoth, C. Hierold, A. Wallraff, and C. Schönenberger, Nat. Commun. **6**, 7165 (2015).